American Mineralogist, Volume 98, pages 2037–2045, 2013

Thermodynamic basis for evolution of apatite in calcified tissues

Sabrina Rollin-Martinet[1,2], Alexandra Navrotsky[3], Eric Champion[2], David Grossin[1] and Christophe Drouet[1,*]

[1]CIRIMAT Carnot Institute, University of Toulouse, UMR 5085 CNRS/INPT/UPS, ENSIACET, 4 allee Emile Monso, 31030 Toulouse cedex 4, France
[2]Université de Limoges, CNRS, SPCTS, UMR 7315, Centre Européen de la Céramique, 12 rue Atlantis, 87068 Limoges cedex, France
[3]Peter A. Rock Thermochemistry Laboratory and NEAT ORU, University of California Davis, 1 Shields Avenue, Davis California 95616, U.S.A.

Abstract

Bone remodeling and tooth enamel maturation are biological processes that alter the physico-chemical features of biominerals with time. However, although the ubiquity of bone remodeling is clear, why is well-crystallized bone mineral systematically replaced by immature nanocrystalline inorganic material? In enamel, a clear evolution is also seen from the first mineral formed during the secretory stage and its mature well-crystalline form, which then changes little in the adult tooth. This contribution provides the thermodynamic basis underlying these biological phenomena. We determined, for the first time, the energetics of biomimetic apatites corresponding to an increasing degree of maturation. Our data point out the progressive evolution of the enthalpy (ΔH_f°) and free energy (ΔG_f°) of formation toward more negative values upon maturation. Entropy contributions to ΔG_f° values remained small compared to enthalpy contributions. ΔH_f° varied from –12 058.9 ± 12.2 to –12 771.0 ± 21.4 kJ/mol for maturation times increasing from 20 min to 3 weeks, approaching the value for stoichiometric hydroxyapatite, –13 431.0 ± 22.7 kJ/mol. Apatite thermodynamic stability increased as its composition moved toward stoichiometry. These findings imply diminishing aqueous solubility of calcium and phosphate ions as well as decreased surface reactivity. Such thermodynamically driven maturation is favorable for enamel maturation since this biomineral is intended to resist external aggressions such as contact with acids. In contrast, maintaining a metastable highly reactive and soluble form of apatite is essential to the effective participation of bone as a source of calcium and phosphate for homeostasis. Therefore our data strongly suggest that, far from being trivial, the intrinsic thermodynamic properties of apatite mineral represent a critical driving force for continuous bone remodeling, in contrast to current views favoring a purely biologically driven cycle. These thermodynamic data may prove helpful in other domains relating, for example, to apatite-based biomaterials development or in the field of (geo)microbiology.

Keywords: Nanocrystalline apatite, hydroxyapatite, bone remodeling, enamel maturation, calorimetry, thermodynamics, metastability, biomimetic

Introduction

Calcified tissues are complex adaptive biomaterials optimized through evolution to provide a union of inorganic and organic constituents to serve both mechanical and biological functions. In particular, one can underline the sophisticated multi-scale architectures found in tooth enamel and bone, which control their mechanical and chemical properties (Weiner and Wagner 1998; Gómez-Morales et al. 2013). Along with morphological aspects, the chemical composition, crystal structure, and microstructure of such apatitic biominerals are adapted to their physiological functions. Enamel, for instance, is intended to protect erupted teeth against external aggressions (thermal, mechanical, chemical), and thus requires in its mature state a high degree of chemical and mechanical stability and low-aqueous solubility. These conditions are met thanks to a chemical composition and other physico-chemical features for mature enamel close to stoichiometric hydroxyapatite (HA, hexagonal, $P6_3/m$ space group) (Bonar et al. 1991). In contrast, far from being inert, bone acts as an ion reservoir allowing for the continual regulation of mineral ion concentrations in body fluids (homeostasis) (Driessens et al. 1986). Therefore, bone mineral should be relatively soluble and should remain highly reactive. Such an increase in solubility and reactivity relative to well-crystallized stoichiometric hydroxyapatite can be attained through nonstoichiometry (ion vacancies) as well as by nanometric crystal dimensions and a low degree of crystallinity (Grynpas 1976).

Without taking into account the presence of secondary elements, the overall composition of biomimetic apatite can generally be satisfactorily described by formulas such as: $Ca_{10-x}(PO_4)_{6-x}(HPO_4)_x(OH)_{2-x}$ (proposed by Winand 1961) or $Ca_{10-x-Z}(PO_4)_{6-x}(HPO_4)_x(OH)_{2-x-2Z}$ (proposed by Kühl and Nebergall 1963), where x and Z depend on factors such as conditions of formation and/or state of aging. The presence of carbonate ions is also observed, especially in mature biominerals (Gómez-Morales et al. 2013), whereas significantly lower carbonate amounts are found in immature ones (Rey et al. 1995). The reactivity of such nanocrystalline apatites is directly connected to specific substructural features: detailed works on such nanocrystalline

* E-mail: Christophe.Drouet@ensiacet.fr

0003-004X/13/1112–2037$05.00/DOI: http://dx.doi.org/10.2138/am.2013.4537

apatite compounds, mostly based on spectroscopic studies (Roufosse et al. 1984; Rey et al. 1989a, 1990; Lu et al. 2000; Kaflak and Kolodziejski 2008), reveal the presence of non-apatitic ionic environments located within a calcium phosphate hydrated layer on the surface of the nanocrystals, whether of synthetic or of biological origin (Cazalbou et al. 2004a; Rey et al. 1989b). This type of complex substructure can probably be related to the mode of formation of apatites (Cazalbou et al. 2004b), which enclose a large number of ions per unit formula and for which the kinetics of crystallization is slow.

The surface layer has been shown to be mostly composed of divalent ions (e.g., Ca^{2+}, HPO_4^{2-}…) that are rather labile and can be easily and rapidly exchanged (within a few minutes) by other ions from the surrounding fluid (Eichert et al. 2008). Ion exchange isotherms with Langmuir-like features are generally seen (Drouet et al. 2008). Also, the presence of this layer plays a key role in the adsorption of (bio)molecules (Ouizat et al. 1999), and such adsorption phenomena sometimes involve a simultaneous release of surface ions (Errassifi et al. 2010). The presence of this layer generally leads to amorphous-like features on electron microscopy analyses (Sakhno et al. 2010), and solid state NMR data also distinguish between the less-ordered surface ionic environments and bulk species (Wu et al. 2002; Jager et al. 2006; Kaflak and Kolodziejski 2008).

The preparation of synthetic analogs to biological apatites (i.e., mimicking at the same time compositional, crystallographic, and microstructural features) has been made possible at the laboratory scale using "mild" synthetic conditions, generally through precipitation at room temperature and physiological pH (Rey et al. 1989b; Cazalbou et al. 2004a, 2004b; Drouet et al. 2009). Variations in synthesis protocols, especially modification of temperature, pH, and/or maturation time prior to precipitate filtration, significantly alter the structural and chemical characteristics of the nanocrystals (Vandecandelaere et al. 2012). An increase of maturation time (aging in solution) leads to an increase in mean crystallite dimensions as well as a progressive evolution of the chemical composition toward the stoichiometry of hydroxyapatite [$Ca_{10}(PO_4)_6(OH)_2$, denoted "HA"] (Cazalbou et al. 2004a), much like what is observed in vivo for enamel maturation between the initial stages of formation (during the secretory stage by ameloblast cells) and its mature state (Rey et al. 1995; Gómez-Morales et al. 2013). Also, a decrease in surface reactivity, measured either by ion exchange or adsorption, has been noticed for crystals matured for increasing periods of time in an aqueous medium (Ouizat et al. 1999; Eichert et al. 2008). In the case of bone, several works have reported the modification in mineral composition and in the amount of non-apatitic surface species upon aging, with an increase of the amount of carbonate and a decrease of the HPO_4 content (Kühl and Nebergall 1963; Legros et al. 1987; Rey et al. 1991a, 1995). During this aging process, some ions of the surface layer are likely to be incorporated into the apatitic core of the nanocrystals and the overall surface area decreases. These changes may then limit ion exchange which plays a key role in physiological pathways (Neuman et al. 1956, 1968; Pak and Bartter 1967; Johnson et al. 1970; Fernandez-Gavarron 1978; Neuman and Neuman 1985).

Although apatite nanocrystal maturation/aging has been the object of much investigation, no quantification of the energetics of biomimetic apatite compounds nor of their aging can be found in the literature to the best of our knowledge; as only thermodynamic data for stoichiometric coarsely crystalline apatitic compounds are available (Jemal et al. 1995; Jemal 2004; Ben Cherifa and Jemal 2004). The object of this contribution is to investigate the energetic evolution of precipitated biomimetic apatite during aging, based on solution calorimetric studies coupled with careful characterization and chemical analyses, and to relate the energetics to the behavior of apatite nanocrystal biominerals, linked in particular to enamel maturation and to bone remodeling. This study was carried out on non-carbonated apatites, thus more specifically addressing the first stages of biomineral maturation processes (Rey et al. 1995).

Materials and methods

Synthesis of nanocrystalline apatite compounds

Biomimetic (non-carbonated) nanocrystalline apatite compounds were prepared by precipitation from mixing aqueous solutions of di-ammonium hydrogenphosphate (0.6 M) and calcium nitrate (0.3 M), at 22 °C and at pH = 7.2 close to the physiological value. The excess of phosphate ions in solution, relative to the formation of hydroxyapatite, provides an internal pH buffer without any additives in the precipitating medium. After rapid mixing (1 min), the precipitates were left to mature (aging in solution) for different periods of time, namely 20 min, 3 h, 1 day, 3 days, 5 days, 1 week, and 3 weeks. Then the precipitates were filtered on Büchner funnel, thoroughly washed with deionized water and freeze-dried (freeze-dryer set to –80 °C, residual pressure 10 mbar).

Stoichiometric HA was prepared following a previously reported protocol (Raynaud et al. 2002). Briefly, the precipitation was carried out under reflux at 90 °C and pH = 8.5 from adding dropwise a solution of di-ammonium phosphate into a solution of calcium nitrate. The synthesis was carried out under argon atmosphere to avoid atmospheric contamination, especially of CO_2. The reactants were used in stoichiometric proportions, in the presence of ammonia for pH stabilization. The mixture was aged for 90 min prior to filtration on Büchner funnel and washing with deionized water. The precipitate was then oven-dried at 80 °C for 24 h and calcined at 1000 °C for 15 h.

β-TCP was obtained by calcining at 900 °C for 16 h some amorphous calcium phosphate [am-$Ca_3(PO_4)_2$] prepared by rapid precipitation from calcium nitrate (0.36 M) and di-ammonium hydrogenphosphate (0.154 M) solutions under strongly alkaline conditions (pH = 10) after the protocol proposed by Heughebaert and Montel (1982).

Characterization techniques

Powder X-ray diffraction (XRD) was performed for crystal structure identification, using a Bruker D8 Advance diffractometer with the monochromatic Cu$K\alpha_1$ radiation (λ = 1.5406 Å, step 0.021°). XRD profile fitting was performed using the JANA 2006 software. The crystallite mean length was estimated by applying the Hosemann and Vogel model (Vogel and Hosemann 1970) to the (002) and (004) planes, as this model takes into account the possible existence of non-negligible crystal disorder effects.

Fourier transform infrared (FTIR) was used, in transmission mode, for complementary phase identification. The experiments were carried out on a Perkin Elmer 1600 spectrometer, in the wavenumber range 400–4000 cm^{-1} and at 4 cm^{-1} resolution.

The calcium content of the solids was determined by complexometry with EDTA (Charlot 1974). The relative error is 0.5%. Orthophosphate ionic contents (PO_4^{3-}, HPO_4^{2-}) were measured by colorimetry (λ = 460 nm) based on the yellow phospho-vanado-molybdenum complex $VO_3[P(Mo_3O_{10})_4]$ formed in acidic conditions (Gee and Dietz 1953). Measurements were carried out in quartz holder with an UV-visible Hitachi Instruments U-1100 single beam spectrophotometer. These orthophosphate ion titrations have a relative error of 0.5%. The amount of the protonated species HPO_4^{2-} ions is derived by comparing titrations carried out before and after calcining the samples at 600 °C for 1 h, which leads to the condensation of HPO_4^{2-} ions into pyrophosphate ions ($P_2O_7^{4-}$) that do not form the yellow complex, as detailed by Gee and Dietz (1953).

The thermal behavior of the differently matured apatites was followed by thermogravimetry (TG) analyses carried out in air on a Setaram SETSYS Evolu-

tion apparatus (heating rate 2.5 °C/min, temperature range 20–900 °C). Water contents of the starting powders were derived from the weight loss observed in the temperature range 20–300 °C.

High-temperature oxide melt solution calorimetry

High-temperature drop solution calorimetry was carried out in a Tian-Calvet twin calorimeter, as described in detail by Navrotsky (1977, 1997). Drop solution enthalpies were measured by dropping 5 mg pressed pellets of material directly from room temperature, 298 K, into the molten solvent in the calorimeter, 973 K. Sodium molybdate ($3Na_2O{\cdot}4MoO_3$) was selected as appropriate solvent for this work based on earlier data (Ushakov et al. 2001) showing that all phosphorus was retained in the melt after dropping P_2O_5 or other phosphate-containing compounds.

Total calorimetric reaction times during calorimetry were in all cases <1 h. The shape of the calorimetric peaks was consistent with rapid sample dissolution during the first few minutes of reaction. The end of the reaction was judged by the return of the baseline to its initial value. A minimum of 8 values were obtained for each composition, and uncertainties are two standard deviations from the mean value. During the experiments, air was flushed through the gas space above the melt (~80 mL/min) so as to accelerate the elimination of gases produced (H_2O or CO_2).

Results and Discussion

Characterization

The calcium phosphate apatite samples prepared in this study with various maturation times (Table 1) were characterized by complementary techniques. TEM observations showed that all prepared samples exhibited a platelet morphology (see typical example of the 1 day maturation sample on Fig. 1). This plate-like morphology is characteristic of that of bone apatite (morphological biomimetism) as reported in the literature (Johansen and Parks 1960). Powder XRD patterns exhibited diffraction peaks that could all be attributed to a hydroxyapatite-like phase (hexagonal, $P6_3/m$ space group, PDF card 09-0432) as indicated in Figure 2. The samples are characterized by a low degree of crystallinity, as for natural bone mineral (Gómez-Morales et al. 2013) or immature enamel crystals (Rey et al. 1995; Gómez-Morales et al. 2013). The crystallinity of these synthetic materials progressively increases upon maturation in accordance with previous data (Neuman et al. 1956; Vandecandelaere et al. 2012). This increased degree of crystallinity is indicated by the better resolution of the XRD patterns, which is especially visible for peaks (002), (004), and (310) in the $2\theta = 28–36°$ range. XRD peak broadening analysis, using the Hosemann and Vogel model (Vogel and Hosemann 1970), led to the evaluation of mean crystallite dimensions. The longest mean crystallite dimension is accessible from analysis of the (002) and (004) peaks and increases from ca. 12 to 27 nm for maturation times ranging from 20 min to 3 weeks, thus confirming the nanocrystalline character of these samples.

FTIR analyses further confirm the apatitic nature of the samples (Fig. 3a). Detailed observation of the spectra reveal, as expected from previous studies (Rey et al. 2007a, 2007b), the presence of non-apatitic contributions, especially in the ν_4PO_4 vibration region (400–800 cm^{-1}) and more specifically at 535 cm^{-1} (non-apatitic HPO_4^{2-} ions) and 617 cm^{-1} (non-apatitic PO_4^{3-}). For more mature samples, the libration band of apatitic OH^- at 631 cm^{-1} becomes visible (see Fig. 3b, illustrating an apatite matured for 1 week).

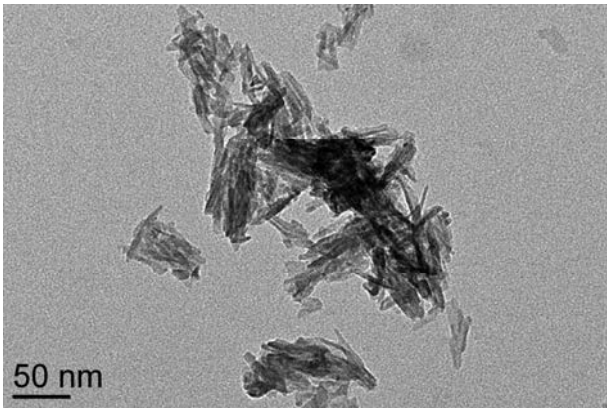

Figure 1. TEM micrograph for a biomimetic apatite sample matured for 1 day.

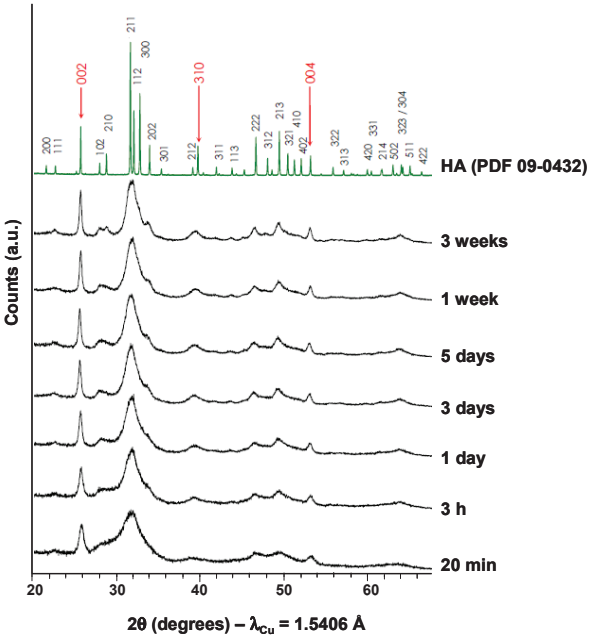

Figure 2. XRD pattern for nanocrystalline apatite samples with various maturation times. (Color online.)

Table 1. Chemical composition of apatite samples (estimated uncertainty on each ion content: 0.5%)

Maturation time	Ca/P mole ratio	Value of Z*	Contents (moles per apatite unit formula*)				
			Ca^{2+}	PO_4^{3-}	HPO_4^{2-}	OH^-	H_2O
20 min	1.43	0.42	8.55	4.97	1.03	0.13	5.94
3 h	1.42	0.43	8.54	4.97	1.03	0.12	4.18
1 day	1.44	0.24	8.64	4.88	1.12	0.39	3.60
3 days	1.48	0.39	8.86	5.25	0.75	0.46	3.53
5 days	1.49	0.12	8.92	5.04	0.96	0.80	3.21
1 week	1.49	0.17	8.94	5.11	0.89	0.77	2.86
3 weeks	1.54	0.07	9.21	5.28	0.72	1.15	3.28

* Considering Kühl and Nebergall's (1963) expression $Ca_{10-x-Z}(PO_4)_{6-x}(HPO_4)_x(OH)_{2-x-2Z}$.

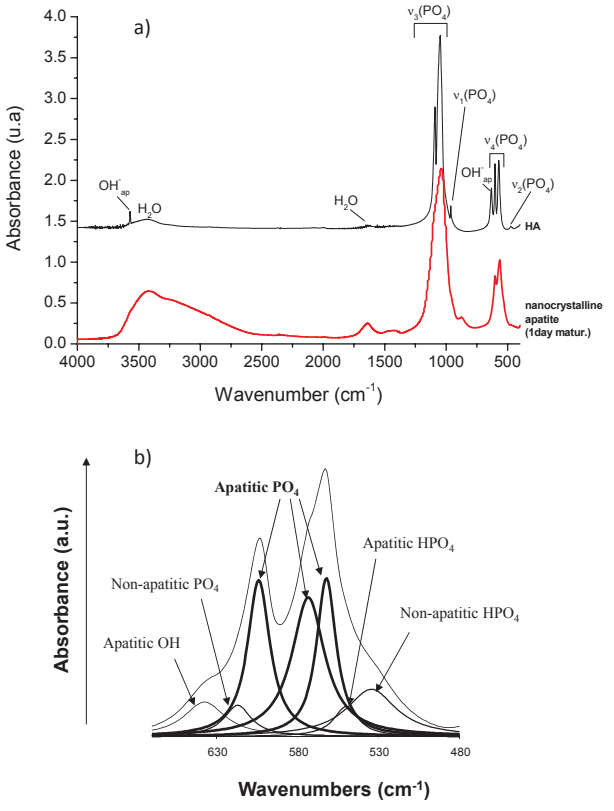

FIGURE 3. (**a**) FTIR spectrum for a nanocrystalline apatite sample matured 1 day, (**b**) detail in the ν_4PO_4 vibration region for a sample matured 1 week. (Color online.)

The presence of non-apatitic contributions substantiates again the biomimetic character of these apatite compounds (Eichert et al. 2008), and it stresses their departure from the structure and composition of coarse hydroxyapatite "reference" material.

Calcium and phosphate titrations along with thermal analyses and the condition of electroneutrality enabled the determination of the contents of each ionic species and water in every sample produced with increasing maturation times. The determination of HPO_4/PO_4 relative amounts is made possible for such apatite samples due to the absence of carbonate ions, therefore enabling one to determine accurate chemical compositions needed for calorimetric evaluations. Indeed, the HPO_4/PO_4 balance is generally drawn from orthophosphate titration, by comparing results obtained before and after heating the samples at 600 °C (which decomposes HPO_4^{2-} into non-titrable pyrophosphates $P_2O_7^{4-}$), while carbonate ions may interfere with these titration methods by partially reacting with HPO_4^{2-} ions through reactions such as $CO_3^{2-}+2HPO_4^{2-} \rightarrow CO_2+2PO_4^{3-}+H_2O$ (Eichert et al. 2008).

The water content has been assessed from the measured weight loss observed by thermogravimetric analyses between 20 and 300 °C (see Supplementary Figure AR1[1]) as this range corresponds to the release of such associated water molecules from apatite nanocrystals (Banu 2005). The chemical composition of the samples is reported in Table 1. The calcium and hydroxyl contents increase with maturation time, while the HPO_4^{2-} content decreases. These variations produce a progressive evolution of the chemical composition of the samples toward the stoichiometry of hydroxyapatite. This evolution can also be monitored by following the Ca/P mole ratio, which increases here from 1.42 to 1.54 (±0.02). The amount of associated water molecules also decreases as aging in solution progresses. These trends suggest the progressive disappearance of the hydrated non-apatitic surface layer from the nanocrystals.

Although the chemical formula $Ca_{10-x}(PO_4)_{6-x}(HPO_4)_x(OH)_{2-x}$ is often used to describe nonstoichiometric apatites, it shows some limitations when applied to the current analytical data, especially for short maturation times. In contrast the formula proposed by Kühl and Nebergall (1963), $Ca_{10-x-Z}(PO_4)_{6-x}(HPO_4)_x(OH)_{2-x-2Z}$, involving lower calcium and hydroxide contents, satisfactorily describes the overall chemical composition of the biomimetic apatite phases prepared in this work, and the values of Z are also indicated in Table 1. Z was indeed found to become significant for the most immature samples. Taking into account the presence of "n" moles of water per unit formula in the freeze-dried samples, the complete chemical formula thus becomes $Ca_{10-x-Z}(PO_4)_{6-x}(HPO_4)_x(OH)_{2-x-2Z}\cdot nH_2O$.

Enthalpies of formation

The determination of the enthalpy of formation from the oxides of these apatites ($\Delta H_{f,oxides}$) from measured enthalpies of drop solution (ΔH_{ds}) requires the application of a thermodynamic cycle, indicated in Table 2. This cycle uses the experimental value of ΔH_{ds} measured for each hydrated apatite corresponding to various maturation stages, as well as the enthalpies of drop solution of calcium carbonate $CaCO_3$ (calcite) and phosphorus oxide P_2O_5. The latter was determined previously by Ushakov et al. (2001). Calcium carbonate was preferred to calcium oxide in this study taking into account the difficulty to keep anhydrous CaO, which has a tendency to partially transform into calcium hydroxide. The enthalpies of formation of the apatites from the elements, ΔH_f°, can then be calculated by adding the appropriate literature values of enthalpies of formation of the binary oxides from their elements. The application of this cycle to reference compounds, namely β-tricalcium phosphate (β-TCP) and stoichiometric hydroxyapatite (Table 3), led to ΔH_f° values of –4090.2 ± 10.6 kJ/mol and –13 431.0 ± 22.7 kJ/mol, respectively. These numbers are in good agreement (within ~0.7%) with values reported in the literature (Robie and Hemingway 1995) [–4120.8 ± 5.0 kJ/mol and –13 477.0 ± 10.0 kJ/mol, respectively, the latter value being expressed for the unit formula $Ca_{10}(PO_4)_6(OH)_2$ rather than $Ca_5(PO_4)_3OH$)], thus validating this cycle and measurements.

The application of the cycle then leads (Table 3) to the evaluation of the standard enthalpies of formation of the apatite samples as prepared (hydrated) as well as those of the apatite phases themselves (anhydrous). As indicated in Table 2, the latter were obtained by considering hydration water molecules as thermodynamically equivalent to liquid water, as is often the case for hydrated phases in which H_2O is not tightly bound and can be released below 300 °C (Drouet and Navrotsky 2003).

The enthalpy values thus obtained, either relative to the elements or to the oxides, become more negative (exothermic) as mat-

[1] Deposit item AM-13-1107, Supplemental Figures. Deposit items are stored on the MSA web site and available via the American Mineralogist Table of Contents. Find the article in the table of contents at GSW (ammin.geoscienceworld.org) or MSA (www.minsocam.org), and then click on the deposit link.

uration progresses. ΔH_f° varies from –12 058.9 ± 12.2 to –12 771.0 ± 21.4 kJ/mol for maturation times increasing from 20 min to 3 weeks (Fig. 4a), thus approaching the value for stoichiometric HA, i.e., –13 431.0 ± 22.7 kJ/mol. The ΔH_f° = f(t) curve follows a monotonic, nearly exponential trend with faster changes during the first 3 days of aging and slower progression beyond this stage. This trend is then found to parallel the evolutions (in the opposite direction) of the Ca^{2+} and OH^- ion contents of the maturing apatite phases (see Supplementary Figure AR2). Based on these findings, the enthalpy of formation of a nanocrystalline apatite phase appears to be direcly related to its calcium and hydroxide contents. Indeed, the plot of ΔH_f° vs. Ca^{2+} or OH^- ion content shows roughly linear variations (see Supplementary Figure AR3), with fit parameters taking into account the cumulated experimental uncertainties (R^2 = 0.886 and 0.937, respectively). Since the calcium content can be determined easily by techniques such as EDTA complexometry, ICP-AES or atomic absorption spectroscopy, and is often reported in literature studies (as opposed to the hydroxide content which is less easily accessible) we report here specifically the equation found for the linear fit obtained vs. the apatite calcium content: ΔH_f° (apatite) = –903.8·[Ca^{2+} content] – 4426.7, in kJ/mol, and the relative error on ΔH_f° (apatite) can be estimated to be 1.0% (see Fig. 4b). These findings thus allow us to unveil, for the first time quantitatively, the direct correlation between the energetics of formation of biomimetic apatites and their ionic contents. Since the amount of calcium is directly linked to the number of cationic vacancies, and similarly the hydroxide content to the amount of anionic vacancies, ΔH_f° is found to fundamentally depend on the apatite maturation state: the system gets more energetically favorable (more exothermic ΔH_f°) as there are fewer crystal "defects" in the structure. The linear variation of enthalpy with Ca^{2+} or OH^- contents also supports the fact that this trend is rather independent on the distribution of the calcium ions between the surface hydrated layer and the apatitic core: it thus allows one to extend the use of this prevision trend to other synthesis scenarios leading to nanocrystalline apatites as final product. It should be noted that the contribution of the non-apatitic chemical environments to the energetics cannot at present be separated from the overall energetic trend. Finally, these findings provide weak evidence that clustering or ordering of such defects does not occur with major energetic consequences.

Entropies and Gibbs free energies

Entropy values for nonstoichiometric nanocrystalline apatites are not accessible from the literature. Data reported for well-crystallized stoichiometric apatitic compounds such as hydroxy-,

TABLE 2. Thermodynamic cycle used in the calculations of ΔH_f°

Reactions		ΔH
(1)	$Ca_{10-x-Z}(PO_4)_{6-x}(HPO_4)_x(OH)_{2-x-2Z}(H_2O)_n \rightarrow (10-x-Z)$ CaO (soln, 973) + 3 P_2O_5 (soln, 973) + (1–Z+n) H_2O (g, 973)	ΔH_{ds} (apatite, hydrated)
	Reactions from oxides	
(2)	$CaCO_3$ (s, 298) → CaO (soln, 973) + CO_2 (g, 973)	$\Delta H_{ds}(CaCO_3)$
(3)	CO_2 (g, 298) → CO_2 (g, 973)	$\Delta H_{hc}[CO_2$ (g)]
(4)	P_2O_5 (s, 298) → P_2O_5 (soln, 973)	$\Delta H_{ds}(P_2O_5)$
(5)	H_2O (g, 298) → H_2O (g, 973)	$\Delta H_{hc}[H_2O$ (g)]
(6)	H_2O (l, 298) → H_2O (g, 298)	$\Delta H^\circ_{vap,298}[H_2O$ (l)]
	Reactions from elements	
(7)	Ca (s, 298) + C (s, 298) + ⅗ O_2 (g, 298) → $CaCO_3$ (s, 298)	$\Delta H_f^\circ(CaCO_3)$
(8)	C (s, 298) + O_2 (g, 298) → CO_2 (g, 298)	$\Delta H_f^\circ[CO_2$ (g)]
(9)	Ca (s, 298) + ½ O_2 (g, 298) → CaO (s, 298)	ΔH_f°(CaO)
(10)	2 P (s, 298) + ⅝ O_2 (g, 298) → P_2O_5 (s, 298)	$\Delta H_f^\circ(P_2O_5)$
(11)	H_2 (g, 298) + ½ O_2 (g, 298) → H_2O (g, 298)	$\Delta H_f^\circ[H_2O$ (g)]
	Formation of nanocrystalline apatites from the oxides	
(12)	(10–x–Z) CaO (s, 298) + 3 P_2O_5 (s, 298) + (2–x–2Z+n) H_2O (l, 298) → $Ca_{10-x-Z}(PO_4)_{6-x}(HPO_4)_x(OH)_{2-x-2Z}(H_2O)_n$	$\Delta H^\circ_{f,oxides}$ (apatite)
Therefore:	$\Delta H^\circ_{f,oxides}$ (apatite) = $-\Delta H_1$ + (10–x–Z) ΔH_{ds}(CaO) +3 ΔH_4 + (2–x–2Z+n) ΔH_5 + (2–x–2Z+n) ΔH_6 = – ΔH_1 + (10–x–Z) [ΔH_2+ΔH_7–ΔH_9–ΔH_8–ΔH_3] +3 ΔH_4 + (2–x–2Z+n) ΔH_5 + (2–x–2Z+n) ΔH_6	
	Formation of nanocrystalline apatites from the elements	
(13)	(10–x–Z) Ca (s, 298) + 6 P (s, 298) + (1–Z+n) H_2 (g, 298) + (26–x–2Z+n)/2 O_2 (g, 298) → $Ca_{10-x-Z}(PO_4)_{6-x}(HPO_4)_x(OH)_{2-x-2Z}(H_2O)_n$	ΔH_f° (apatite, hydrated)
Therefore:	ΔH_f° (apatite, hydrated) = – ΔH_1 + (10–x–Z) ΔH_2 + (10–x–Z) ΔH_7 – (10–x–Z) ΔH_3 – (10–x–Z) ΔH_8 + 3 ΔH_4 + 3 ΔH_{10} + (1–Z+n) ΔH_5 + (1–Z+n) ΔH_{11} ≅ ΔH_f° (apatite, anhydrous) + n $\Delta H_f^\circ[H_2O$ (l)]	

TABLE 3. Experimental ΔH_{ds} values and derived $\Delta H_{f oxides}$ and ΔH_f° for nanocrystalline apatites and for reference compounds HA and β-TCP (±S.D.)

Sample	ΔH_{ds} (kJ/mol)	ΔH_f° (compound) (kJ/mol)	298 K, 1 atm	
		Reference compounds		
β-TCP	267.3 ± 9.7 (6)*	–4090.2 ± 10.6		
HA stoich.	1027.7 ± 21.4 (11)	–13431.0 ± 22.7		
Sample	ΔH_{ds} (kJ/mol)	ΔH_f° (apatite, hydrated) (kJ/mol)	$\Delta H_{f\ oxides}$ (kJ/mol)	**ΔH_f° (kJ/mol)**
		Nanocrystalline apatites		
20 min	1197.7 ± 10.0 (10)	–13756.8 ± 12.2	–1952.2 ± 12.5	**–12058.9 ± 12.2**
3 h	1198.2 ± 15.0 (9)	–13370.7 ± 16.5	–2073.9 ± 16.8	**–12174.9 ± 16.5**
1 day	1241.7 ± 9.5 (8)	–13393.4 ± 11.8	–2152.7 ± 12.1	**–12364.4 ± 11.8**
3 days	1088.6 ± 9.1 (9)	–13352.3 ± 11.5	–2032.8 ± 11.8	**–12342.1 ± 11.5**
5 days	1077.4 ± 5.1 (9)	–13373.3 ± 8.7	–2030.5 ± 9.2	**–12457.0 ± 8.7**
1 week	1137.2 ± 9.1 (10)	–13362.2 ± 11.5	–2119.5 ± 11.9	**–12546.1 ± 11.5**
3 weeks	1172.8 ± 20.2 (9)	–13708.7 ± 21.4	–2141.3 ± 21.6	**–12771.0 ± 21.4**

* Numbers in parentheses indicate the number of drop solution calorimetry experiments.

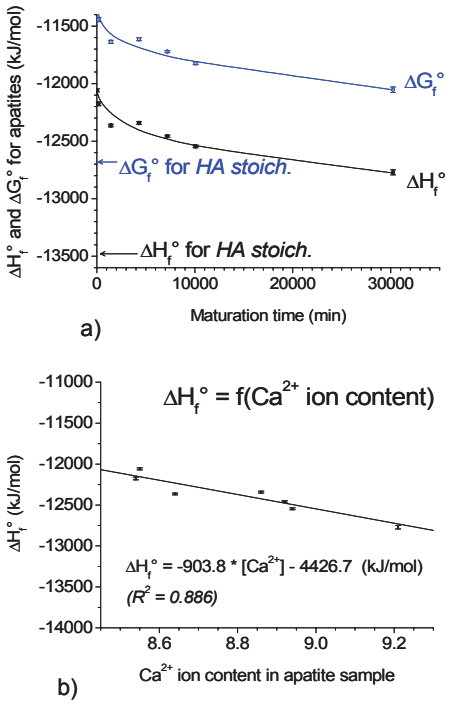

FIGURE 4. (**a**) Evolution of ΔH_f° and ΔG_f° for nanocrystalline apatites vs. maturation time in solution (uncertainties are two standard deviations, S.D., of the mean), and (**b**) linear fit for ΔH_f° = f(Ca^{2+} content). (Color online.)

fluor-, and chlor-apatites are on the contrary available (Jemal et al. 1995; Jemal 2004; Ben Cherifa and Jemal 2004), and a calculation reveals that, in all cases, the entropy contributions of $T\Delta S_f^\circ$ represent only a minor proportion of the Gibbs free energy of formation $\Delta G_f^\circ = \Delta H_f^\circ - T\Delta S_f^\circ$ (of the order of 6%, see Supplementary Figure AR4[1]) compared to the enthalpy contribution ΔH_f°. Therefore the relative stability of such compounds, which are theoretically assessed by comparing ΔG_f° values, can also be reached in a more direct way by comparing the enthalpies of formation accessed by calorimetry. The data reported in Figure 4a therefore suggest that the relative stability of biomimetic apatites increases as maturation progresses, evolving toward the level of stoichiometric hydroxyapatite (without reaching it though).

We obtain a better estimate of the entropy of nanocrystalline apatites by considering the following reaction

$$(9–x)CaO_{(s,298)} + 3P_2O_{5(s,298)} + (1–Z)Ca(OH)_{2(s,298)} \rightarrow Ca_{10–x–Z}(PO_4)_{6–x} + (HPO_4)_x(OH)_{2–x–2Z(s,298)}. \quad (1)$$

Since this reaction only involves solid phases, the corresponding entropy change, ΔS°_{react}, is expected to be close to zero. Considering $\Delta S^\circ_{react} = 0$, $T = 298$ K and entropy values for CaO, P_2O_5, and $Ca(OH)_2$ from thermodynamic databases (Robie and Hemingway 1995), this reaction leads for stoichiometric HA (x = Z = 0) to the standard entropy S°(HA) = 769.5 J/(mol·K). This value is in reasonable agreement (within 1.5%) with the value 780.8 J/(mol·K) reported in the literature (Robie and Hemingway 1995) [expressed for the unit formula $Ca_{10}(PO_4)_6(OH)_2$] thus supporting this estimation method. In a similar way, the entropy S° of each nanocrystalline apatite from this work was evaluated, as well as the corresponding standard entropy of formation from the elements ΔS_f° (Table 4). The Gibbs free energies of formation ΔG_f° could then also be derived, at 298 K, from the ΔH_f° and ΔS_f° values. These data show again that the entropy contributions to the ΔG_f° values are small compared to enthalpy contributions, and that the Gibbs free energy becomes more negative (favorable) as the system gets more mature (Fig. 4a). This conclusion probably still holds even if one adds the contribution of a possible configurational entropy resulting from the location of defects in the structure, but this contribution cannot be calculated accurately. Note that entropy contributions may presumably also be approximated using computational methods. However, such calculations would require good knowledge of stuctural features, while the exact location of ions contained in the hydrated layer on such biomimetic apatites is still essentially undertermined.

A major variation of ΔG_f° similar to that in ΔH_f° is found during the first days of maturation in solution, while the decrease in ΔG_f° becomes less pronounced beyond a few days. A plot of ΔG° vs. calcium content again leads to a linear trend (see Supplementary Figure AR3), corresponding to the equation ΔG_f° (apatite) = –843.6 * [Ca^{2+} content] – 4204.5 (in kJ/mol, $R^2 = 0.880$, relative error estimated to 1.1%). This equation then allows one to draw predictive estimates of the value of ΔG_f° for other calcium phosphate nanocrystalline apatites, based on the determination of their calcium content.

Apatite maturation energetics

It is desirable to estimate the variation in free energy of maturation $\Delta G_{maturation}$(i→f), corresponding to the maturation process in solution transforming an apatite from an initial maturation stage "i" to a more advanced stage "f". To this aim, it is necessary to take into account the thermodynamic data for the aqueous ions incorporated or released during this maturation process in solution. This task is however more difficult than it may appear at first sight. Indeed, the maturation process is a complex phenomenon where not only the chemical composition evolves

TABLE 4. Evaluation of S°, ΔS_f°, and ΔG_f° for nanocrystalline apatites matured between 20 min and 3 weeks, and for stoichiometric HA (±S.D.)

Sample	At 298 K			
	Estimated S° J/(mol·K) [±20 J/(mol·K)]	Estimated ΔS_f° J/(mol·K) [±20 J/(mol·K)]	Recall of ΔH_f° kJ/mol	Corresponding ΔG_f° kJ/mol
Nanocrystalline apatite compounds:				
20 min	695.2	–2469	–12058.9 ± 12.2	–11323.1 ± 12.2
3 h	694.6	–2467	–12174.9 ± 16.5	–11439.7 ± 16.5
1 day	706.6	–2512	–12364.4 ± 11.8	–11616.0 ± 11.8
3 days	708.2	–2507	–12342.1 ± 11.5	–11595.0 ± 11.5
5 days	722.9	–2565	–12457.0 ± 8.7	–11692.6 ± 8.7
1 week	721.4	–2558	–12546.1 ± 11.5	–11783.9 ± 11.5
3 weeks	736.5	–2607	–12771.0 ± 21.4	–11994.2 ± 21.4
Stoichiometric HA	769.5	–2704	–13477 ± 10	–12674.2 ± 10

toward stoichiometry, but also where secondary reactions such as dissolution-reprecipitation may play a role. However, the global change in chemical composition during maturation can probably be considered as a dominant phenomenon, since the overall ion content can significantly change upon maturation as illustrated by Table 1, which is bound to quantitatively impact the compounds thermodynamic properties.

Considering the simplified scenario where only the global change in apatite composition is taken into account, it is possible to determine in particular the sign of $\Delta G_{maturation}(i \rightarrow f)$ based on a modeled maturation reaction. The increase in Ca/P ratio that accompanies the observed evolution toward stoichiometry could theoretically either be explained by an additional incorporation of Ca^{2+} ions (increase of numerator) or by a release of phosphate ions in the medium (decrease of denominator), or both. However, the concentration of free calcium ions in solution is likely to be extremely low due to the large excess of phosphate ions in the synthesis medium or to the presence of numerous calcium-complexing entities in body fluids in vivo (phosphates, carbonates and protein ionic species). Therefore, the possibility to incorporate additional Ca^{2+} ions from the solution appears unlikely. In contrast, the release of phosphate ions from the solid to the solution appears much more probable, especially as a protonated form which is stable under physiological pH. Since phosphate ions from the non-apatitic surface layer are mostly protonated as HPO_4^{2-}, while the amount of HPO_4^{2-} in the solid decreases upon maturation (in both synthetic and biological apatites) (Rey et al. 1991b; Cazalbou et al. 2004a) in favor of non-protonated PO_4^{3-}, the release of phosphate as $H_2PO_4^-$ appears as the most probable route, which may be described by the following scheme, involving proton hopping between two surface HPO_4^{2-} ions

$$2HPO_{4\,(solid)}^{2-} \rightarrow H_2PO_{4\,(released\ in\ solution)}^{-} + PO_{4\,(solid)}^{3-} \quad (2)$$

Since this departure of anionic $H_2PO_4^-$ ions from the solid would lead to a decrease in negative charges, it has to be compensated by a simultaneous incorporation of OH^- ions. This was indeed found experimentally by the increased hydroxylation of apatites upon maturation (Table 1). In this context, the global reaction scheme describing the change in composition during the maturation process may probably be written as

$$\text{Apatite in state "i"} + \delta_1 H_2O_{(liq)} \rightarrow \text{Apatite in state "f"} + \delta_2 H_2PO_{4(aq)}^- + \delta_3 H_{(aq)}^+ \quad (3)$$

where the chemical species $H_2O_{(liq)}$ and $H^+_{(aq)}$ have been preferred to the direct involvement of $OH^-_{(aq)}$ ions, due to the neutral pH where such maturations were carried out.

The variation in Gibbs free energy accompanying this reaction can be written as $\Delta G_{maturation}(i \rightarrow f) = \Delta G^\circ_{maturation}(i \rightarrow f) + RT \cdot \ln(K)$ where K, the equilibrium constant, is given by the activity product: $[H_2PO^-_{4(aq)}]^{\delta 2} \cdot [H^+_{(aq)}]^{\delta 3}$. Based on the data in Table 4 and on thermodynamic data (Wagman et al. 1982; Robie and Hemingway 1995) for $H_2O_{(liq)}$ and $H_2PO^-_{4(aq)}$, the values of $\Delta G^\circ_{maturation}(i \rightarrow f)$ were calculated at 298 K for various maturation stages "f" relative to the maturation of 20 min taken as reference (initial state "i"). Also, under physiological conditions (considering pH = 7.4 and $(H_2PO_4^-) \cong 10^{-4}$ M), the values of the $RT \cdot \ln(K)$ term for each sample were determined. The obtained values of $\Delta G_{maturation}$ (at 298 K) are plotted in Figure 5. The dispersion of the points is probably linked to the simplistic scenario considered here, not taking into account secondary surface reaction in particular. Interestingly, the value of $\Delta G_{maturation}$ is found to be negative in all cases, ranging from 0 to -117 ± 23 kJ/mol, with the most negative value corresponding to evolution toward coarse stoichiometric HA (corresponding to -185 ± 15 kJ/mol). These findings give a quantitative background for biomimetic calcium phosphate apatite aging (studied here on synthetic samples over a period of 3 weeks maturation).

The spontaneous character of this maturation process can thus be considered as a thermodynamic driving force explaining the inexorable evolution of nonstoichiometric apatite nanocrystals (e.g., found in immature enamel and in young bone) toward more stable states. Such states are characterized by: (1) a composition closer to stoichiometry, and (2) an associated decrease in surface reactivity and solubility. This stabilization (in terms of both thermodynamics and kinetics) is advantageous in the case of enamel maturation, taking into account the final functions of this biomineral in vivo (i.e., resistance to external aggressions of various natures including chemical). On the contrary, it is not beneficial in the case of bone which needs to remain relatively soluble and reactive (i.e., able to exchange ions with surrounding fluids, and/or to undergo dissolution/reprecipitation phenomena upon remodeling). Our findings thus suggest that bone remodeling has a strong thermodynamic basis. Indeed, according to our data, the metastable apatite composing newly formed bone matter is thermodynamically driven to inevitably transform into a more stable, less soluble, and less reactive state, with lower surface area, minimized non-apatitic surface layer, and fewer reactive surface sites. Such lowered surface reactivity was for example observed in model experiments run on synthetic nanocrystalline apatite and on chicken bone (Cazalbou et al. 2004a).

Thus the maturation of bone apatite crystals with time is bound to lead to limited capability in body fluids homeostasis. Therefore, the above-quantified thermodynamic driving force (negative $\Delta G_{maturation}$) along which reactive but immature apatite nanocrystals evolve toward more mature but less reactive states could be seen as a physical-chemical (rather than purely biologi-

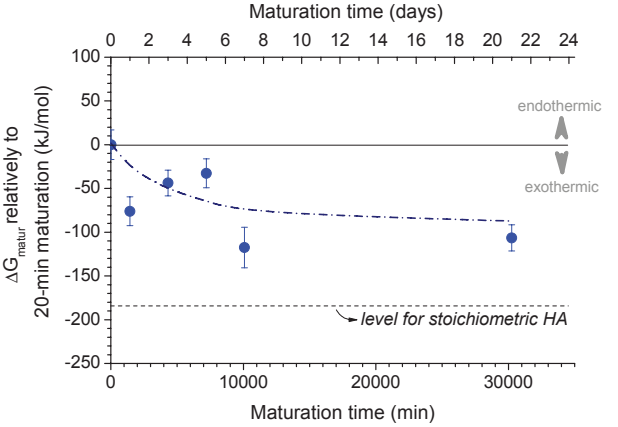

FIGURE 5. Evolution of $\Delta G_{maturation}(i \rightarrow f)$ vs. maturation time, taking the 20 min matured sample as initial state. (Color online.)

cal) basis explaining the need for bone to be regularly remodeled. Then, such remodeling does not only allow skeletal growth from infancy to adulthood as well as self-repair after bone injury (healing of bone tissue microfractures linked to pathological or traumatic events), but it is a "necessity" in view of conserving highly reactive bone biomineral crystals capable of playing their role in homeostasis (e.g., as a participation in the stabilization of calcium, magnesium, strontium, and phosphate concentrations in body fluids). Bone remodeling, which "resets" the maturation process, at the biological cost of the energy and nutrients required for it, is thus favorable and necessary to the organism.

In addition to enabling the estimation of $\Delta G_{maturation}$, the determination of free energies of formation ΔG_f° for such apatite compounds can be used for other thermodynamic calculations. One obvious other example concerns the evaluation of the solubility product of such biomimetic apatites as a function of their maturation state. The question of solubility is indeed relevant when dealing with enamel formation or bone remodeling processes. In the case of hydroxyapatite, the dissolution equilibrium can be described by the reaction

$$Ca_{10}(PO_4)_6(OH)_2 + 2H^+_{(aq)} \leftrightarrow 10Ca^{2+}_{(aq)} + 6PO^{3-}_4 + 2H_2O_{(liq)}. \quad (4)$$

The variation of free energy ΔG°_{disso} accompanying this reaction is linked to the solubility product K_{sp} by the equation

$$\Delta G^\circ_{disso} = -2.303 \cdot RT \cdot \log(K_{sp}) = 2.303 \cdot RT \cdot pK_{sp}. \quad (5)$$

Considering the experimental compositions found in this work, the strict application of this equation at 298 K leads to pK_{sp} values ranging from 96 to 113 (see details in Supplementary Figure AR5). As a general tendency, these calculations suggest that apatite solubility decreases as maturation progresses, tending toward the value for stoichiometric HA (McDowell et al. 1977) [pK_{sp}(HA) = 117]. However, several literature studies (Hsu et al. 1994; Baig et al. 1996; Chhettry et al. 1999) have pointed out noticeable differences between the apparent solubility of nonstoichiometric calcium phosphate apatites and their theoretical value, despite long periods of stabilization in solution, thus showing that the system did not reach the true thermodynamic equilibrium. This phenomenon depicts a situation where dissolution (relatively rapid at first) has essentially stopped and where nucleation/growth processes are not discernable, over the temporal scale of the experiments. Also the non-constancy of the solubility product for such compounds was unveiled by these studies, as it was found to depend on the fraction of mineral dissolved. This behavior, referred to as metastable equilibrium of solubility (MES), was then found to be related to the existence of microstrains (Higuchi et al. 1984) within the constitutive non-ideal crystals. Nanocrystalline biological and biomimetic apatites exhibit a non-homogeneous chemical composition as the nanocrystals are constituted of an apatitic core surrounded by a non-apatitic surface layer. In these conditions, the observation of altered apparent solubilities—as compared to theoretical values—is rather unsurprising. Due to the incongruence of the dissolution of such nanocrystalline compounds, it should be kept in mind that such pK_{sp} values drawn from ΔG°_{disso} may only be considered for pointing out the decreasing solubility of biomimetic apatites upon aging. These pK_{sp} values should however be considered with caution for determining precise calcium and phosphate concentrations in surrounding solutions: for this purpose, experimental solubility tests remain the best approach.

IMPLICATIONS

The inexorable evolution of immature apatite crystals with time is advantageous in the case of enamel where increased stability and lower solubility are beneficial to the "protection" functionality of this biomineral. In contrast, a similar thermodynamically driven evolution of apatite is deleterious for bone mineral, which plays a key role in the regulation of body fluid ionic concentrations in vivo through homeostasis. These results strongly suggest that bone remodeling could be seen as a thermodynamic necessity to eliminate the "too stable" and poorly bioactive aged apatite crystals in favor of the neo-formation of immature, less stable, and highly reactive nanocrystals. The time-dependent evolution of apatite-based calcified tissues such as bone or enamel could thus be dictated—at least in great part—by a thermodynamic driving force, despite the current emphasis on a mostly biologically driven process. Our data strongly support this new interpretation, with a major role played by mineral thermodynamics.

Beside implications of these thermodynamic data for solubility behavior of nanocrystalline biomimetic apatites, these findings are bound to find other implications. In the domain of ectopic (abnormal or untypical) calcifications, several mineral compounds may be observed in vivo (e.g., apatite, pyrophosphate, whitlockite, and struvite). Specific reasons for their formation are not yet clearly determined. Yet, thermodynamic stabilities are probably involved in the persistence or transformations of such ectopic mineralizations. Biomaterials for bone replacement based on nanocrystalline apatites show great promise due to their high-surface reactivity. However, any synthesis or post-synthesis step (e.g., sterilization), which may involve humid conditions and/or heating should be considered cautiously and with good understanding of nanocrystallie apatite physic-chemistry, since further evolution of the apatite and/or phase transformations may then come into play. Finally, thermodynamic data on such calcium phosphate systems may prove useful in other domains such as (geo)microbiology (e.g., calcifications occurring inside eukaryotic cells) (Raven and Knoll 2010) or link to the evolution of life on Earth (e.g., evolution from carbonate-based shells to phosphate-based skeletons).

ACKNOWLEDGMENTS

The authors thank the French Agence Nationale de la Recherche (ANR) for funding in the scope of the NanoBiocer program (ANR-07-BLAN-0373), as well as the Institut National Polytechnique de Toulouse (INPT) and the France Berkeley Fund (FBF) for co-funding. The authors also thank O. Trofymluk, K. Lilova, and A. V. Radha for experimental support.

REFERENCES CITED

Baig, A.A., Fox, J.L., Hsu, J., Wang, Z.R., Otsuka, M., Higuchi, W.I., and LeGeros, R.Z. (1996) Effect of carbonate content and crystallinity on the metastable equilibrium solubility behavior of carbonated apatites. Journal of Colloid and Interface Science, 179, 608–617.

Banu, M. (2005) Mise en forme d'apatites nanocristallines: ceramiques et ciments. Ph.D. Institut National Polytechnique de Toulouse (INPT), Toulouse, France.

Ben Cherifa, A., and Jemal, M. (2004) Enthalpy of formation and mixing of calcium-cadmium phosphoapatites. Phosphorus Research Bulletin, 15, 113–118.

Bonar, L.C., Shimizu, M., Roberts, J.E., Griffin, R.G., and Glimcher, M.J. (1991) Structural and composition studies on the mineral of newly formed dental enamel—A chemical, X-ray diffraction, and p-31 and proton nuclear magnetic resonance study. Journal of Bone and Mineral Research, 6, 1167–1176.

Cazalbou, S., Combes, C., Eichert, D., Rey, C., and Glimcher, M.J. (2004a) Poorly crystalline apatites: Evolution and maturation in vitro and in vivo. Journal of Bone and Mineral Metabolism, 22, 310–317.

Cazalbou, S., Eichert, D., Drouet, C., Combes, C., and Rey, C. (2004b) Biological mineralisations based on calcium phosphate. Comptes Rendus Palevol, 3, 563–572.

Charlot, G. (1974). Chimie Analytique Quantitative, 2. Masson, Paris.

Chhettry, A., Wang, Z.R., Hsu, J., Fox, J.L., Baig, A.A., Barry, A.M., Zhuang, H., Otsuka, M., and Higuchi, W.I. (1999) Metastable equilibrium solubility distribution of carbonated apatite as a function of solution composition. Journal of Colloid and Interface Science, 218, 57–67.

Driessens, F.C.M., Vandijk, J.W.E., and Verbeeck, R.M.H. (1986) The role of bone mineral in calcium and phosphate homeostasis. Bulletin Des Societes Chimiques Belges, 95, 337–342.

Drouet, C., and Navrotsky, A. (2003) Synthesis, characterization, and thermochemistry of K-Na-H_3O jarosites. Geochimica et Cosmochimica Acta, 67, 2063–2076.

Drouet, C., Carayon, M., Combes, C., and Rey, C. (2008) Surface enrichment of biomimetic apatites with biologically-active ions Mg^{2+} and Sr^{2+}: A preamble to the activation of bone repair materials. Materials Science and Engineering C, 28, 1544–1550.

Drouet, C., Bosc, F., Banu, M., Largeot, C., Combes, C., Dechambre, C., Estournes, C., Raimbeaux, G., and Rey, C. (2009) Nanocrystalline apatites: From powders to biomaterials. Powder Technology, 190, 118–122.

Eichert, D., Drouet, C., Sfihi, H., Rey, C., and Combes, C. (2008) Nanocrystalline apatite based biomaterials: Synthesis, processing and characterization. In J.B. Kendall, Ed., Biomaterials Research Advances, 93–143. Nova Science Publisher, New York.

Errassifi, F., Menbaoui, A., Autefage, H., Benaziz, L., Ouizat, S., Santran, V., Sarda, S., Lebugle, A., Combes, C., Barroug, A., Sfihi, H., and Rey, C. (2010) Adsorption on apatitic calcium phosphates: applications to drug delivery. Advances in Bioceramics and Biotechnologies, 218, 159–174.

Fernandez-Gavarron, F. (1978) The dynamic equilibrium of calcium. In A.P. E. Pina and V. Chagoya de Sanchez, Eds., Temas Biochimicos Actuales, p. 41–67. Universidad Nacional Autonoma, Mexico City.

Gee, A., and Dietz, V.R. (1953) Determination of phosphate by differential spectrophotometry. Analytical Chemistry, 25, 1320–1324.

Gómez-Morales, J., Iafisco, M., Delgado-López, J.M., Sarda, S., and Drouet, C. (2013) Progress on the preparation of nanocrystalline apatites and surface characterization: Overview of fundamental and applied aspects. Progress in Crystal Growth and Characterization of Materials, 59, 1–46.

Grynpas, M. (1976) Crystallinity of bone mineral. Journal of Materials Science, 11, 1691–1696.

Heughebaert, J.C., and Montel, G. (1982) Conversion of amorphous tricalcium phosphate into apatitic tricalcium phosphate. Calcified Tissue International, 34, S103–S108.

Higuchi, R., Bowman, B., Freiberger, M., Ryder, O.A., and Wilson, A.C. (1984) DNA-sequences from the Quagga, an extinct member of the horse family. Nature, 312, 282–284.

Hsu, J., Fox, J.L., Higuchi, W.I., Powell, G.L., Otsuka, M., Baig, A., and Legeros, R.Z. (1994) Metastable equilibrium solubility behavior of carbonated apatites. Journal of Colloid and Interface Science, 167, 414–423.

Jager, C., Welzel, T., Meyer-Zaika, W., and Epple, M. (2006) A solid-state NMR investigation of the structure of nanocrystalline hydroxyapatite. Magnetic Resonance in Chemistry, 44, 573–580.

Jemal, M. (2004) Thermochemistry and relative stability of apatite phosphates. Phosphorus Research Bulletin, 15, 119–124.

Jemal, M., Bencherifa, A., Khattech, I., and Ntahomvukiye, I. (1995) Standard enthalpies of formation and mixing of hydroxyapatites and fluorapatites. Thermochimica Acta, 259, 13–21.

Johansen, E., and Parks, H.F. (1960) Electron microscopic observations on the 3 dimensional morphology of apatite crystallites of human dentine and bone. Journal of Biophysical and Biochemical Cytology, 7, 743–746.

Johnson, A.R., Armstrong, W.D., and Singer, L. (1970) The exchangeability of calcium and strontium of bone in vitro. Calcified Tissue Research, 6, 103–112.

Kaflak, A., and Kolodziejski, W. (2008) Kinetics $^{1}H \rightarrow {}^{31}P$ NMR cross-polarization in bone apatite and its mineral standards. Magnetic Resonance in Chemistry, 46, 335–341.

Kühl, G., and Nebergall, W.H. (1963) Hydrogenphosphat- und Carbonatapatite. Zeitschrift für anorganische und allgemeine Chemie, 324, 313–320.

Legros, R., Balmain, N., and Bonel, G. (1987) Age-related changes in mineral of rat and bovine cortical bone. Calcified Tissue International, 41, 137–144.

Lu, H.B., Campbell, C.T., Graham, D.J., and Ratner, B.D. (2000) Surface characterization of hydroxyapatite and related calcium phosphates by XPS and TOF-SIMS. Analytical Chemistry, 72, 2886–2894.

McDowell, H., Gregory, T.M., and Brown, W.E. (1977) Solubility of $Ca_5(PO_4)_3OH$ in the system $Ca(OH)_2$-H_3PO_4-H_2O at 5, 15, 25, and 37 °C. Journal of Research of the National Bureau of Standards, Section A: Physics and Chemistry, 81A, 273–281.

Navrotsky, A. (1977) Progress and new directions in high-temperature calorimetry. Physics and Chemistry of Minerals, 2, 89–104.

——— (1997) Progress and new directions in high temperature calorimetry revisited. Physics and Chemistry of Minerals, 24, 222–241.

Neuman, W.F., and Neuman, M.W. (1985) Blood: bone calcium homeostasis. Shika Kiso Igakkai Zasshi, 24, 272–281.

Neuman, W.F., Toribara, T.Y., and Mulryan, B.J. (1956) The surface chemistry of bone. 9. Carbonate-phosphate exchange. Journal of the American Chemical Society, 78, 4263–4266.

Neuman, W.F., Terepka, A.R., Canas, F., and Triffitt, J.T. (1968) The cycling concept of exchange in bone. Calcified Tissue Research, 2, 262–270.

Ouizat, S., Barroug, A., Legrouri, A., and Rey, C. (1999) Adsorption of bovine serum albumin on poorly crystalline apatite: Influence of maturation. Materials Research Bulletin, 34, 2279–2289.

Pak, C.Y.C., and Bartter, F.C. (1967) Ionic interaction with bone mineral. I. Evidence for an isoionic calcium exchange with hydroxyapatite. Biochimica et Biophysica Acta, 141, 401–409.

Raven, J.A., and Knoll, A.H. (2010) Non-skeletal biomineralization by eukaryotes: matters of moment and gravity. Geomicrobiology Journal, 27, 572–584.

Raynaud, S., Champion, E., Bernache-Assollant, D., and Thomas, P. (2002) Calcium phosphate apatites with variable Ca/P atomic ratio I. Synthesis, characterisation and thermal stability of powders. Biomaterials, 23, 1065–1072.

Rey, C., Collins, B., Goehl, T., Dickson, I.R., and Glimcher, M.J. (1989a) The carbonate environment in bone mineral—A resolution-enhanced Fourier-transform infrared spectroscopy study. Calcified Tissue International, 45, 157–164.

Rey, C., Lian, J., Grynpas, M., Shapiro, F., Zylberberg, L., and Glimcher, M.J. (1989b) Non-apatitic environments in bone mineral: FT-IR detection, biological properties and changes in several disease states. Connective Tissue Research, 21, 267–273.

Rey, C., Shimizu, M., Collins, B., and Glimcher, M.J. (1990) Resolution-enhanced Fourier-transform infrared spectroscopy study of the environment of phosphate ions in the early deposits of a solid phase of calcium phosphate in bone and enamel, and their evolution with age. 1. Investigations in the ν_4 PO_4 domain. Calcified Tissue International, 46, 384–394.

Rey, C., Beshah, K., Griffin, R., and Glimcher, M.J. (1991a) Structural studies of the mineral phase of calcifying cartilage. Journal of Bone and Mineral Research, 6, 515–525.

Rey, C., Renugopalakrishnan, V., Collins, B., and Glimcher, M.J. (1991b) Fourier-transform infrared spectroscopy study of the carbonate ions in bone mineral during aging. Calcified Tissue International, 49, 251–258.

Rey, C., Hina, A., Tofighi, A., and Glimcher, M.J. (1995) Maturation of poorly crystalline apatites: Chemical and structural aspects in vivo and in vitro. Cells and Materials, 5, 345–356.

Rey, C., Combes, C., Drouet, C., Lebugle, A., Sfihi, H., and Barroug, A. (2007a) Nanocrystalline apatites in biological systems: characterisation, structure and properties. Materialwissenschaft und Werkstofftechnik, 38, 996–1002.

——— (2007b) Physico-chemical properties of nanocrystalline apatites: Implications for biominerals and biomaterials. Materials Science and Engineering C, 27, 198–205.

Robie, R.A., and Hemingway, B.S. (1995) Thermodynamic properties of minerals and related substances at 298.15 K and 1 bar (10^5 Pascals) pressure and at higher temperatures. U.S. Geological Survey Bulletin, 2131, p. 461.

Roufosse, A.H., Aue, W.P., Roberts, J.E., Glimcher, M.J., and Griffin, R.G. (1984) Investigation of the mineral phases of bone by solid-state ^{31}P magic angle sample spinning nuclear magnetic-resonance. Biochemistry, 23, 6115–6120.

Sakhno, Y., Bertinetti, L., Iafisco, M., Tampieri, A., Roveri, N., and Martra, G. (2010) Surface hydration and cationic sites of nanohydroxyapatites with amorphous or crystalline surfaces: A comparative study. Journal of Physical Chemistry C, 114, 16640–16648.

Ushakov, S.V., Helean, K.B., Navrotsky, A., and Boatner, L.A. (2001) Thermochemistry of rare-earth orthophosphates. Journal of Materials Research, 16, 2623–2633.

Vandecandelaere, N., Rey, C., and Drouet, C. (2012) Biomimetic apatite-based biomaterials: On the critical impact of synthesis and post-synthesis parameters. Journal of Materials Science: Materials in Medicine, 23, 2593–2606.

Vogel, W., and Hosemann, R. (1970) Evaluation of paracrystalline distortions from line broadening. Acta Crystallographica, A26, 272–277.

Wagman, D.D., Evans, W.H., Parker, V.B., Schumm, R.H., Halow, I., Bailey, S.M., Churney, K.L., and Nuttall, R.L. (1982) The NBS tables of chemical thermodynamic properties. Selected values for inorganic and C_1 and C_2 organic substances in SI units. Journal of Physical and Chemical Reference Data, 11 (supp. 2), 1–392.

Weiner, S., and Wagner, H.D. (1998) The material bone: Structure mechanical function relations. Annual Review of Materials Science, 28, 271–298.

Winand, L. (1961) Etude physico-chimique du phosphate tricalcique hydrate et de l'hydroxylapatite. Annales de Chimie (Paris), 13th series, 6, 941–967.

Wu, Y.T., Ackerman, J.L., Kim, H.M., Rey, C., Barroug, A., and Glimcher, M.J. (2002) Nuclear magnetic resonance spin-spin relaxation of the crystals of bone, dental enamel, and synthetic hydroxyapatites. Journal of Bone and Mineral Research, 17, 472–480.

Manuscript received March 14, 2013
Manuscript accepted July 7, 2013
Manuscript handled by Daniel Vielzeuf